ARTICLE

JAAS
www.rsc.org/jaas

Remote LIBS with ultrashort pulses: characteristics in picosecond and femtosecond regimes†

Ph. Rohwetter,[a] J. Yu,*[b] G. Méjean,[b] K. Stelmaszczyk,[a] E. Salmon,[b] J. Kasparian,[b] J.-P. Wolf[b] and L. Wöste[a]

[a]*Fachbereich Physik der Freien Universität Berlin, Institut für Experimentalphysik, Arnimallee 14, D-14195 Berlin, Germany*
[b]*Laboratoire de Spectrométrie Ionique et Moléculaire (LASIM), UMR CNRS 5579, Université Claude Bernard-Lyon 1, 43, Bd. du 11 Novembre 1918, F-69622 Villeurbanne Cedex, France. E-mail: jinyu@lasim.univ-lyon1.fr*

Received 15th December 2003, Accepted 23rd February 2004
First published as an Advance Article on the web 4th March 2004

Using a container-integrated mobile femtosecond terawatt laser system with integrated detection unit (Teramobile), we have demonstrated remote laser-induced breakdown spectroscopy (R-LIBS) on copper and aluminium samples with targets located at 25 m away from the container. The ability of our laser system to generate pulses in the femtosecond, picosecond and nanosecond regimes allowed us to perform direct comparisons between these three pulse durations. The dependence of the fluorescence signal on laser pulse energy showed a nonlinear behavior with a threshold, which is consistent with the previous observations for laser ablation. Such nonlinear behavior leads to a dependence of the LIBS signal on the temporal-spectral shape of the laser pulse. We showed especially that the transform-limited pulse does not optimize the fluorescence. A properly applied chirp allows an increase of the LIBS signal. Understanding and optimization of the chirp effect would improve the detection limit of the LIBS using a femtosecond laser (Femto-LIBS) and lead to a larger detection distance. Furthermore the use of pulse shaping should enhance the detection specificity for the cases of spectral overlapping between several elements to be identified.

1 Introduction

Laser-induced breakdown spectroscopy (LIBS) (known also as laser-induced plasma spectroscopy, LIPS) is a versatile analytical method which involves the interaction of a target with an intense laser pulse and the spectral analysis of the fluorescence emission from the generated plasma plume.[1–4] Since plasma production is possible with a sample without any preparation, LIBS is applied on gas, liquid, solid or particle state samples.[5] The applications of the LIBS technique are very broad.[5] They cover environmental monitoring (soil contaminations, air or water quality surveillance…), industrial processing by materials analysis (mineral resources, impurities, quality control, sorting…), biomedical studies (teeth, bones…), military and safety needs, space exploration, and art works analysis. Recent progress has enabled the LIBS techniques to go from laboratory to field applications: long-range open-path LIBS[6] as well as mobile LIBS[7] devices have been realized.

The detection limit of the LIBS technique actually lies in the range from 1 to 100 ppm for most of the elements,[8,9] much higher compared with other laser-based analytical methods, such as LIDAR (down to the ppb level, but only for gases).[10] Remote detection or element identification with LIBS is further limited by the difficulty of delivering high laser intensities over long distances in order to induce ionisation on the target. Increasing the efficiency and measurement range and lowering the LIBS detection limit are important issues for LIBS applications.

Besides the usual IR (typically Nd:YAG: 1064 nm) and visible (typically doubled Nd:YAG: 532 nm) pulse excitations, UV pulses (typically KrF: 248 nm) have been demonstrated to be able to achieve the same detection limit with much lower laser pulse energy.[11,12] Double-pulse schemes have been proposed to improve the LIBS detection sensitivity. In such configurations, either a pre-ablation air plasma created near the sample surface by a first pulse depletes locally ambient air and enhances the ablation rate of the second pulse,[13,14] or the interaction between the second pulse and the plasma plume generated by the first pulse leads to a more efficient fluorescence emission.[15]

Ultrashort laser pulses with duration in the picosecond or femtosecond ranges represent attractive laser sources to design new and more sensitive LIBS systems. Not only have the advantages of such pulses in laser ablation and laser micromachining been clearly demonstrated with lower ablation threshold and less thermal damages on the sample,[16–18] but also the development of laser diode pumping and of fibre systems promise compact and reliable ultrashort laser sources.[19,20] Recently 100 ps duration pulses obtained using compression by stimulated Brillouin scattering (SBS) has been applied to LIBS.[21] Picosecond or femtosecond pulse induced LIBS has been studied using mode-locked laser systems in laboratory experiments. Some comparisons have been performed in the ultrashort pulse regime with respect to the classical nanosecond regime.[22,23] Remote LIBS (R-LIBS) with pico- or femto-second laser systems had not been demonstrated so far, partially because usual ultrashort laser systems, especially those which deliver high pulse energy (suitable for remote detections), need a well controlled laboratory environment to run properly.

In this paper we show that using a container-integrated mobile terawatt femtosecond laser, together with the associated detection system (telescope, spectrometer, ICCD camera), it is possible to remotely induce and detect LIBS signals with signal to noise ratios allowing analytical applications. Systematic studies have been carried out with standard industry quality metallic samples (copper and aluminium) at a distance of 25 m to characterise the R-LIBS signal in the picosecond and femtosecond regimes. Comparisons are shown with the

† Presented at the Second Euro-Mediterranean Symposium on Laser Induced Breakdown Spectroscopy, Hersonissos, Crete, Greece, September 30th–October 3rd, 2003.

DOI: 10.1039/b316343a

nanosecond regime. The dependences of the R-LIBS signal on the pulse energy and pulse chirp are experimentally studied, showing interesting results. The applications of these effects should lead to a more efficient LIBS with a lower detection limit and longer detection distance. Although a full understanding of the mechanisms involved is not achieved yet, we provide ideas to interpret the observed spectra or dependences. For applications, the obtained experimental data are very useful for the design of new LIBS systems based on ultrafast lasers. These data should also stimulate the development of new theoretical models in order to reach a better understanding of the LIBS in ultrashort and/or ultraintense pulse regimes.

2 Experimental set-up

As shown in Fig. 1, the experimental set-up consisted in two main parts: the laser system and the detection system. The ensemble is called a Teramobile[24] system. Both parts were contained in a standard container of 6 m length and 2.5 m width. The container is transportable and provides a stable environment for a proper operation of the both laser and detection systems under various climatic conditions. Once installed in an experimental site, only standard electricity and water supplies are needed for the stand-alone operation of the Teramobile system.

2.1 Laser system

A detailed description of the laser system can be found elsewhere.[25] Briefly, a commercial chirped-pulse-amplification (CPA)[26] chain (Thales Laser Company) was integrated in a standard container. The laser chain consisted of an oscillator, a stretcher, a regenerative amplifier, a preamplifier, a main amplifier and a compressor. Operating at a wavelength of 795 nm and a repetition rate of 10 Hz, the chain delivered pulses of up to 350 mJ in energy and compressed to 75 fs minimal pulse duration.

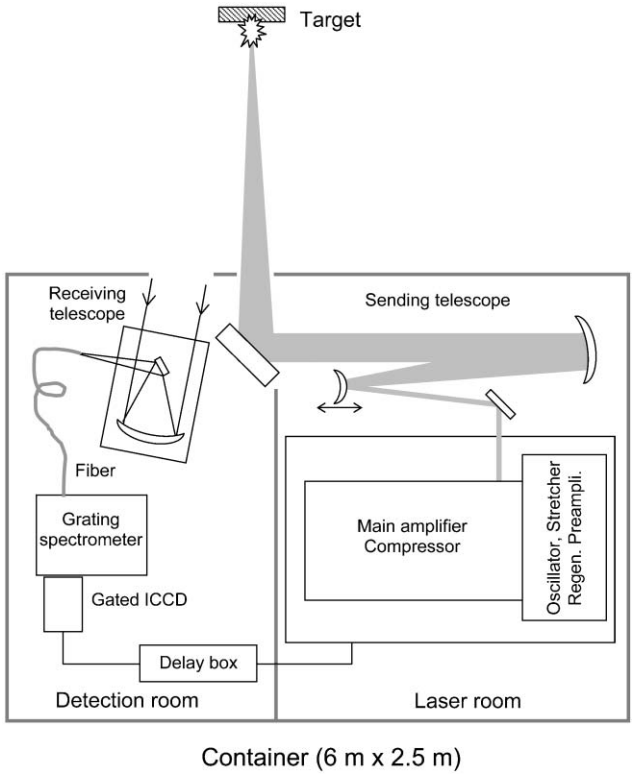

Fig. 1 Schematic diagram of the experimental set-up including the stand-alone container divided inside into a laser room and a detection room, the femtosecond terawatt laser system, the reflective sending telescope, the receiving telescope, the transmitting fibre, the grating spectrometer, the gated ICCD camera, and the synchronization delay generator. The target was located at a distance of 25 m from the container. The output laser beam was focused by the sending telescope with a movable convex mirror to ensure an optimised beam focusing on the target.

One of the gratings in the compressor was mounted on a micro-displacement stage, enabling the control of the pulse duration from sub-100 fs to several ps. In the cases where output pulses were not compressed to their minimal duration, the pulses were temporally chirped. We could get either a positive chirp: the red components preceding the blue ones (the red first), or a negative chirp with a reverse ordering of different spectral components of the pulse (the blue first). The output pulse energy could be varied by rotating a $\lambda/2$ plate associated with a polarizer, without any change in the pulse duration or in the pulse spatial profile. That allowed us to have a change of laser intensity on the samples linearly proportional to the change of the pulse energy.

The same laser provided pulses with 200 ps or 5 ns durations. Picosecond pulses were obtained by bypassing the compressor, while ns pulses were generated when the seeding of the regenerative amplifier by the oscillator pulses was removed. This specific feature of our laser allowed us to compare easily R-LIBS signals in the three pulse duration regimes. We remark that ps pulses were actually long positively chirped pulses with a perfect coherence between different spectral components. Spatial beam profiles for the three above pulse durations were quite similar and presented a flat-top form.

Output pulses were transmitted horizontally into the atmosphere after passing through a three-times beam expander with a convex and a concave mirror (Fig. 1, sending telescope). The convex mirror was mounted on a stepper motor, which precisely set the distance between the two mirrors to focus the output beam at a remote distance. At the output window of the container, the beam diameter was 15 cm. In our experiments, the laser beam was focused on the targets located 25 m away from the container.

2.2 Detection system

For the measurements presented in this paper, the detection system was located beside the laser in the container (Fig. 1). It consisted of a f/5 aperture Newtonian telescope with a primary mirror of 10 cm in diameter. Light collected at the focus of the telescope was coupled into a bundle of fibres with a circular section for the input end and a rectangular section for the output end. The f-number of the fibre output was adapted to the input of a f/8 ($f = 500$ mm) spectrometer (Chromex 500IS/SM). An ICCD camera (Standford Research Inc.) was mounted on the reciprocal plane to record spectra. With a 600 lines mm^{-1} grating, our detection had a resolution of about 0.0862 nm $pixel^{-1}$ on the ICCD. Typically we applied an entrance slit of 100 μm aperture, which led to a final resolution of our detection of 0.34 nm. The ICCD camera was triggered by a photodiode detecting scattered light on the sending mirror due to output laser pulses. The gating of the intensifier of the camera was delayed with respect to the laser pulse by a delay generator (Stanford Research Inc.).

The spectral detectivity of our detection system was measured with a halogen lamp considered as a black-body source at a temperature of 3000 K. The detection system used was sensitive and calibrated between 450 and 950 nm.

The alignment of the detection system was performed with a low energy frequency-doubled YAG laser shooting on a target 25 m away from the container. The visible image of the impact spot of the laser on the target allowed us to set precisely the input end of the fibre on the focal point of the telescope. The initial distance between the laser and the telescope axis was 0.85 m. To increase the signal to noise ratio and to overcome the fluctuations due to laser pulse to pulse jitter, we typically

took spectra with an accumulation of hundreds of laser shots, which represented an accumulation time of typically 0.5 min.

3 Experimental results

In this section the results are presented in the following way: in section 3.1, R-LIBS spectra from copper and aluminium samples are presented. We compare the spectra obtained with femtosecond, picosecond and nanosecond pulses. The decay of the R-LIBS signal as a function of the detection delay is presented in section 3.2. Section 3.3 is devoted to the dependences of the R-LIBS signal on the laser parameters. We especially discuss dependences of the fluorescence yield on the pulse energy and pulse chirp.

3.1 Characteristics of R-LIBS spectra in the natural atmosphere

3.1.1 Remote ablation with femtosecond and picosecond pulses. We used industry-grade copper and aluminium bulk samples without any surface cleaning. Very small aging effects were observed on the copper sample. The recorded LIBS signal stabilized after the first several laser shots. Contrary to copper, the aging effect was clearly observed in aluminium. During the first minutes of laser shooting, the observed spectral intensity varied as a consequence of the surface cleaning by laser pulses. Afterwards the signal stabilized showing only small variations during further laser excitations. Photographs of laser impacts on the sample surfaces are shown in Fig. 2. For the same beam focusing, the laser craters are larger for femtosecond pulses. The observed difference in crater dimensions can be explained by an intensity threshold for laser ablation: the short duration of femtosecond pulses allows even the edge of the beam profile to reach the intensity threshold. For an estimation of the laser intensity deposited on the sample, we use the surface of the crater on the aluminium sample due to femtosecond pulses. The photograph (Fig. 2(b)) shows a surface of about 34 mm^2 (8 mm × 4.2 mm). For the pulse energy of 225 mJ (corresponding to a fluence of 0.66 J cm^{-2}) used to obtain the spectra shown in this section, an intensity of 8.8×10^{12}, 3.3×10^9 and 1.3×10^8 W cm^{-2}, respectively, is associated with the femtosecond, picosecond and nanosecond pulses. It should be noted that these values correspond to averaged intensities (or fluence) over the beam profile. Much higher intensities (or fluences) are reached at the center of the focused spot. Except for the results presented in the section 3.3.2, femtosecond pulses were always compressed to their minimal duration of 75 fs.

From Fig. 2, for picosecond pulses, a polished surface is observed in the center of the craters, testifying the melting phase of the surface following the interaction with a laser pulse. In the literature, temperatures exceeding 3000 K are reported in ns pulse produced plasma,[27] much higher than the melting temperatures of copper (1365 K) and aluminium (930 K). For femtosecond pulses, the observed craters show a rough aspect in the central part, with fringe-like structure (several 100 μm period) for the copper sample.

By weighing the aluminium sample before and after 22 000 shots of femtosecond laser pulses, we found an ablated mass of 0.014 g, which corresponds to an ablation of about 640 ng per femtosecond pulse. This value is quite similar to that found for a thin aluminium film (500 nm thickness) ablated by femtosecond pulses.[28] A mass ablation rate can calculated from the mass removed per pulse (for the pulse parameters of 75 fs duration, focused on a 0.34 cm^2 spot, 150 mJ pulse energy, 5.9×10^{12} W cm^{-2} average intensity), leading to a value of 2.5×10^7 g (cm $s)^{-1}$. This value is more than two orders of magnitude higher than the value for nanosecond pulses at the same intensity.[29,30]

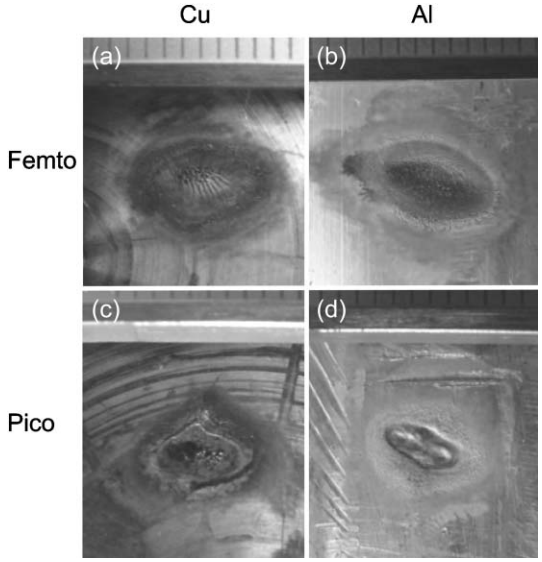

Fig. 2 Photographs showing laser impacts on the targets: femtosecond pulses on the copper (a) and the aluminium (b) samples; picosecond pulses on the copper (c) and the aluminium (d) samples. The scales appearing on the tops of the photographs are in mm. All of the four photographs are presented in the same scale.

3.1.2 Copper spectrum. In Fig. 3 spectra obtained with femtosecond (Fig. 3(a)), and picosecond (Fig. 3(b)) pulses are presented. The delay and the gate width applied on the ICCD camera were 10 ns and 10 μs, respectively, for femtosecond pulses, and 345 ns and 1 μs for picosecond pulses. In the case of

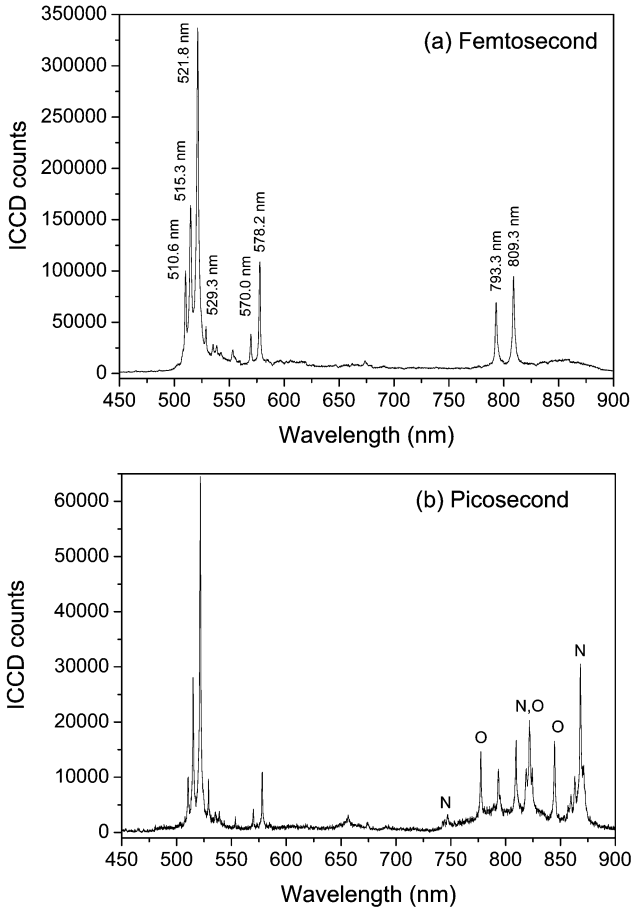

Fig. 3 R-LIBS spectra for the copper sample at 25 m: (a) using 75 fs pulses, (b) using 200 ps pulses. Wavelengths of observed copper lines are indicated in (a), positions of observed atomic oxygen and nitrogen lines are indicated in (b).

femtosecond pulses, 400 laser shots were accumulated for each spectrum, while in the case of picosecond pulses, 150 shots were accumulated. The zero delay is defined as the arrival time of elastically scattered light from the target.

Using femtosecond pulses, atomic copper lines are well observed over a weak continuum. No ionic lines are observed in this spectral range in spite of the presence of ionic lines as indicated by the spectral database provided by the NIST.[31] Using picosecond pulses, additional lines are detected in the range between 700 and 900 nm. These additional lines are identified as belonging to atomic oxygen or atomic nitrogen. Using the NIST database, the corresponding lines are indicated in Fig. 3(b). The presence of these additional lines can be considered as due to a secondary plasma generated by the breakdown in air near the sample surface induced by the fast jet of laser-ablated material.[32] Direct breakdown in air induced by a laser pulse is not considered here, because of the small intensity in a picosecond pulse. The secondary air plasma also indicates a higher temperature in the plasma plumes induced by picosecond pulses than in those due to femtosecond pulses, which is consistent with the observation from the photographs of laser-induced craters. From the application point of view, femtosecond pulses induce a cleaner spectrum independent of the ambient gas, which is an appreciable quality for quick and precise identifications of elements in an unknown environment.

Starting from the signal to noise of the spectrum (521.82 nm line) shown in Fig. 3(a), which can be measured to be 110 (400 laser shots average), we can deduce a signal to noise ratio of 5.5 for a single shot spectrum. A single-pulse analysis capability of about a few 100 ng of copper can thus be expected for a sample at 25 m away from the laser, if we assume a similar mass ablation rate between copper and aluminium. Such an assumption is quite reasonable because similar mass ablation rates between copper and aluminium have been measured in the nanosecond regime.[33]

3.1.3 Aluminium spectrum. In Fig. 4 spectra obtained with femtosecond (Fig. 4(a)), picosecond (Fig. 4(b)) and nanosecond (Fig. 4(c)) pulses are presented. The delay and the gate width applied on the ICCD camera were 345 ns and 10 μs, respectively. 400 shots were accumulated for the femtosecond spectrum and 200 shots for the picosecond and nanosecond ones.

For femtosecond pulses, in the spectral range of the detection, only lines belonging to the molecule AlO were observed (AlO: $B\,^2\Sigma^+ \rightarrow X\,^2\Sigma^+$). No atomic or ionic Al lines were observed in spite of the presence of lines in this spectral range as indicated by the NIST database. The sodium 589 nm line is observed in the spectrum due to a contamination of the aluminium sample by salt.

The detection of the fluorescence of aluminium monoxide in a laser-ablated aluminium plasma has been reported previously with ns pulses.[27,34] AlO molecules are found to be either produced from laser ablation of alumina (Al_2O_3)[27] or formed in a gas-phase chemical reaction of Al vapor with a gas of atomic oxygen.[34] For an aluminium sample exposed in the atmosphere, the surface is quickly oxidized within the interval between two successive laser pulses. Moreover, the highly energetic material jet[32] ablated by a laser pulse produces near the aluminium surface an oxygen plasma, in which Al + O → AlO reactions take place. The absence of atomic and ionic aluminium lines can be explained by either fast oxidization of the aluminium sample surface or fast chemical reaction between Al and O to form AlO. A white-light continuum is also observed in the spectrum, indicating the high temperature reached in the laser-induced plasma.

For picosecond pulses (Fig. 4(b)), in addition to the AlO lines, atomic oxygen and nitrogen lines are observed similarly as for the copper sample. However, two atomic aluminium lines (669.6 and 877.3 nm) are observed in the spectrum. The presence of these lines suggests a post-ablation interaction

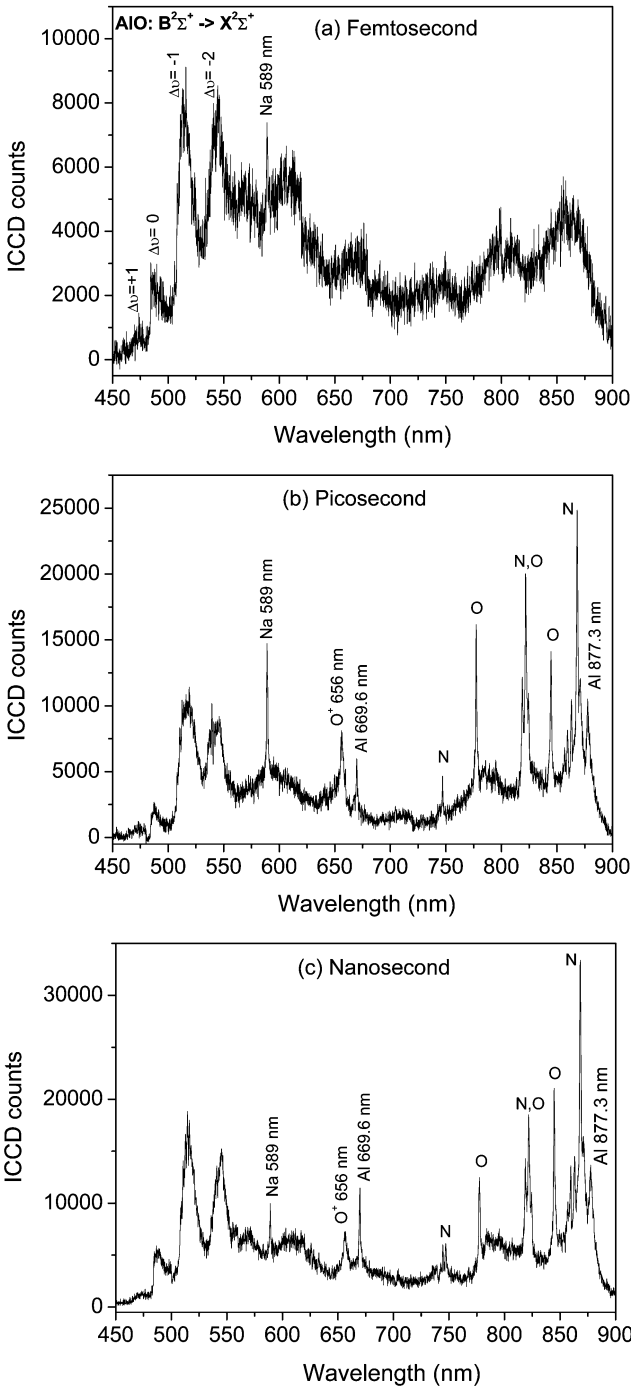

Fig. 4 R-LIBS spectra for the aluminium sample at 25 m: (a) using 75 fs pulses, (b) using 200 ps pulses, (c) using 5 ns pulses. The observed AlO lines belong to the transition $B\,^2\Sigma^+ \rightarrow X\,^2\Sigma^+$ with $\Delta v = 1, 0, -1, -2$. The observed atomic and ionic oxygen and nitrogen lines are indicated in (b) and (c). Note also two Al atomic lines as indicated in (b) and (c).

between the plasma plume and the tailing part of the laser pulse in the picosecond regime. With nanosecond pulses, the spectrum (Fig. 4(c)) has a similar behavior to the picosecond spectrum. This is not really a surprise because as for picosecond pulses, the post-ablation interaction plays an important role in the fluorescence generation in the nanosecond regime.

The signal to noise ratio is smaller for aluminium than for copper because our detection did not allow the measurements of intense Al lines in the blue and UV regions.

3.2 Decay of the R-LIBS signals

The decay of the laser induced fluorescence was studied using 160 mJ femtosecond and picosecond pulses. Spectra were

recorded with a fixed gate width of 10 μs and an increasing detection delay. The large gate width of 10 μs was used to increase the detected signal. However, since the used gate width is larger than the time constant of the LIBS signal decay, the detected signal is related to the integral of the instantaneous fluorescence from the target: $S(\tau) = \int_{\tau}^{\infty} s(t)\mathrm{d}t$, where $s(t)$ is the instantaneous signal at a time t, $S(\tau)$ the integrated signal detected with a delay τ and a gate width much larger than the signal decay time constant. In such a mode of detection, the instantaneous signal $s(t)$ can be extracted from the detected signal $S(\tau)$, by a derivation. Moreover if an exponential decay is assumed, either the instantaneous or integrated fluorescence signals have the same decay time constant. We remark here that the temporal behavior of the fluorescence might also be directly measured by applying a gate width much shorter than the time constant of the signal decay.

Fig. 5 shows normalized line intensities for the copper 510.6 and 515.3 nm lines, and the AlO $B\,^2\Sigma^+ \rightarrow X\,^2\Sigma^+$, $\Delta v = -1$ line induced by femtosecond pulses as a function of the detection delay. We note that the copper atomic lines decay faster than the AlO molecular line. For the two studied copper lines, the decay time constants are slightly different. This difference is not observed for the different AlO lines. For all lines studied, a decay time constant of several μs is observed, which is one order of magnitude longer than previously reported values obtained with low energy femtosecond pulses (1 mJ, 140 fs).[35] This difference indicates different interaction regimes with different fluences for femtosecond pulses.

The results in the picosecond regime are presented in Figs. 6 and 7. In Figs. 6(a) and 7(a), full spectra (with 400 laser shot accumulations), respectively, of copper and aluminium are presented for different delays from 10 ns up to 6 μs. Differential decays are clearly observed between the copper or AlO/Al lines and the air plasma lines. With a large delay, a clean copper or AlO/Al spectrum is observed while air plasma lines almost completely disappear. Line intensities are extracted from the full spectra, and are presented, respectively, in Figs. 6(b) and 7(b) for copper and aluminium, and differential decays are shown clearly between metallic plasma fluorescence and air plasma fluorescence. The observed air plasma lifetime is already much longer than that of the air plasma (in the order of nanoseconds) induced directly by femtosecond laser pulses at the same intensity level as in our experiments.[36]

The generation of a secondary plasma in air in the vicinity of a solid or liquid surface by means of laser ablation provides also a means to chemically analyse the ambient air. An efficient fluorescence generation with a much longer lifetime compared to the direct plasma generation in air is expected.

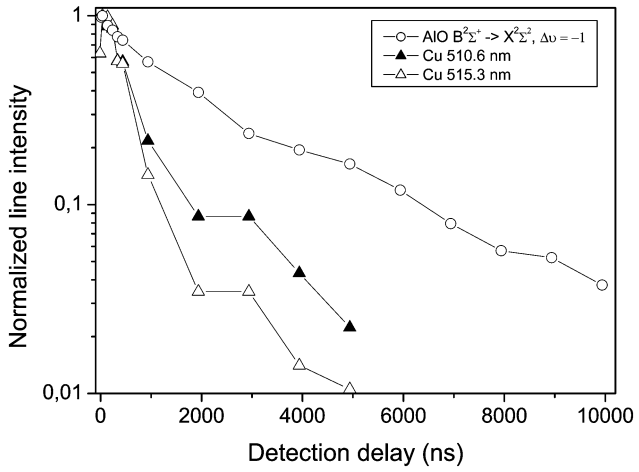

Fig. 5 Normalized spectral line intensities as a function of the detection delay with femtosecond pulse excitation for copper and aluminium.

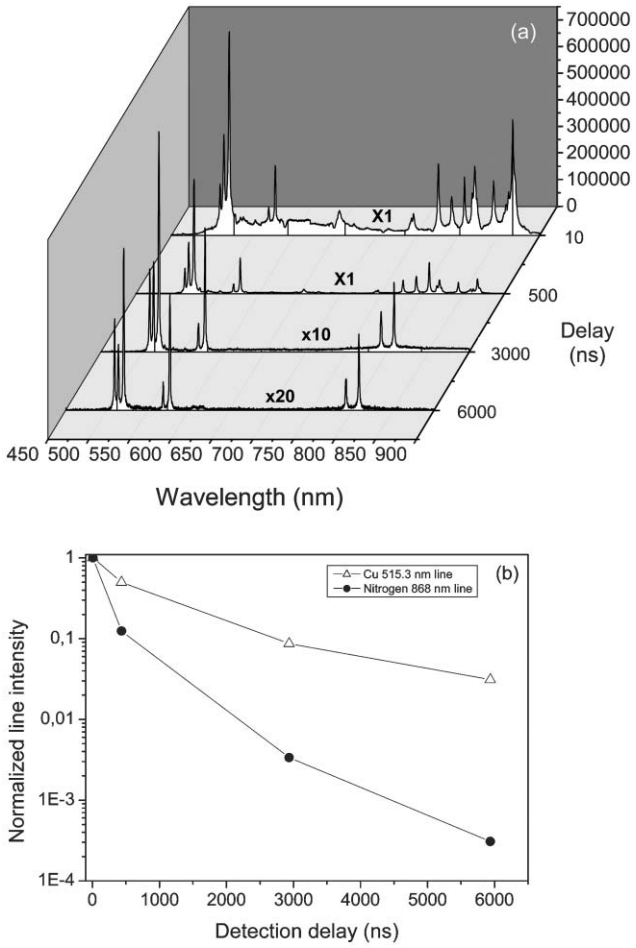

Fig. 6 (a) Full spectra obtained from the cooper target with picosecond pulses at different detection delays. (b) Normalized intensities of the copper 515.3 nm line and the nitrogen 868 nm line as a function of the detection delay.

We conclude for this section, that with ultrashort pulses in the high fluence regime, the induced plasma fluorescence has a lifetime of several μs, which is orders of magnitude longer than the lifetimes in the low fluence regime. Such long fluorescence lifetimes allow the use of slower and less expensive gated detectors to get clean spectra, as well as a long integration time to increase the signal. The air plasma due to the ejection of laser-ablated material could be used to chemically analyse the ambient air with a high sensitivity.

3.3 R-LIBS signal *vs.* laser parameters

3.3.1. Pulse energy dependence. Pulse energy dependence of the R-LIBS signal was investigated in the femtosecond and picosecond regimes. Signals from copper were detected for pulse energies as low as 15 mJ (corresponding to an average fluence of 45 mJ cm^{-2}) in the femtosecond regime.

Fig. 8 shows the intensity of the copper 521.8 nm line in the femtosecond regime as a function of the laser pulse energy. The experimental data fit well with the model of Hashida *et al.*[18] This model takes two contributions into account: 3-photon absorption, and thermal processes involving the thermal energy of the free electrons and the lattice, respectively. The fit parameters yield a threshold of 40 mJ pulse energy for the thermal ablation process, corresponding to an average fluence of 120 mJ cm^{-2} over the beam profile, slightly lower than the 180 mJ cm^{-2} value determined by Hashida *et al.* This slight discrepancy could be due to the different criteria used for the threshold and the imprecision on the beam focus diameter estimation in our experiments. While Hashida *et al.* are interested in laser ablation and characterize threshold as the

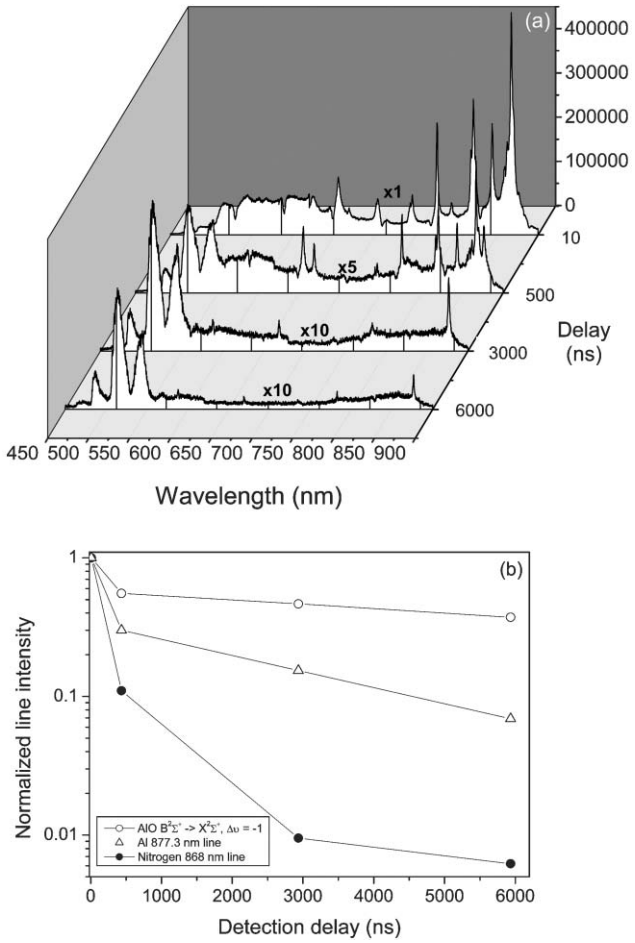

Fig. 7 (a) Full spectra obtained from the aluminium target with picosecond pulses at different delays. (b) Normalized intensities for the AlO $\Delta v = -1$, Al 877.3 nm and nitrogen 868 nm lines as a function of the detection delay.

fluence yielding craters of measurable diameters, we detected fluorescence emission instead. However, like these authors, we find that, above this threshold, the 3-photon excitation has a negligible contribution to the overall signal.

In the picosecond regime with copper, the same treatment yields a threshold value of 100 mJ (300 mJ cm^{-2}), more than twice as high as using femtosecond pulses. This 2.5-fold ratio is similar to that observed by Hashida *et al.* under comparable conditions. Hence, femtosecond pulses exhibit a reduced threshold as compared with picosecond pulses, allowing measurements at lower laser energies, thus limiting damage on the sample. Alternatively, this lower threshold may permit to focus the beam less tightly, opening the way to operate at longer focal lengths. Moreover the fact that we observed a signal with femtosecond pulses significantly below the threshold for thermal ablation shows that, in the low energy regime, the 3-photon excitation is efficient enough to provide a signal. This feature is a unique advantage of femtosecond pulses for R-LIBS, since the 3-photon ionisation threshold for picosecond pulses is above, not below, the threshold for thermal effects.[18]

Similar results were obtained with aluminium, in the AlO $B\,^2\Sigma^+ \rightarrow X\,^2\Sigma^+$, $\Delta v = -1$ line. In the femtosecond regime, the threshold for thermal ablation was determined as 60 mJ (180 mJ cm^{-2}), similar to the value determined by Furukawa and Hashida.[17] The threshold for picosecond pulses is quite comparable, 70 mJ, corresponding to 210 mJ cm^{-2}.

3.3.2. Pulse shape dependence. The temporal-spectral shape is an important parameter for a femtosecond pulse because of its short duration and its large spectral extent in the order of tens of nm. The chirp (linear temporal displacement of the different spectral components of a laser pulse) provides a simple case of pulse shaping. In general, a nonlinear optical process depends on the chirp when excited by a femtosecond pulse, which is basically due to the quantum interference between multiple possible paths for a system to undergo a transition involving several photons (more than one).[37,38] Pulse chirping or more generally pulse shaping (a generalized pulse chirping process that produces an arbitrary temporal-spectral form of a pulse), have been demonstrated to be able to optimise multiphoton transitions in an atomic or molecular system.[38,39] It has also been demonstrated that the transform-limited pulse does not optimise multiphoton transitions in an atomic system.[39] In our experiments, we generalize this property to the interaction between a chirped femtosecond pulse and a metallic sample. We demonstrated clearly, for the first time to our knowledge, that the transform-limited pulse does not produce an optimal LIBS signal, and that the optimisation occurs for a properly chirped pulse. We mention here that shaped femtosecond pulses have been used to improve laser ablation performances with successful results.[40]

Experimentally we studied the evolution of the R-LIBS signal as a chirp was applied to femtosecond pulses with an energy fixed at 250 mJ. For copper as well as for aluminium

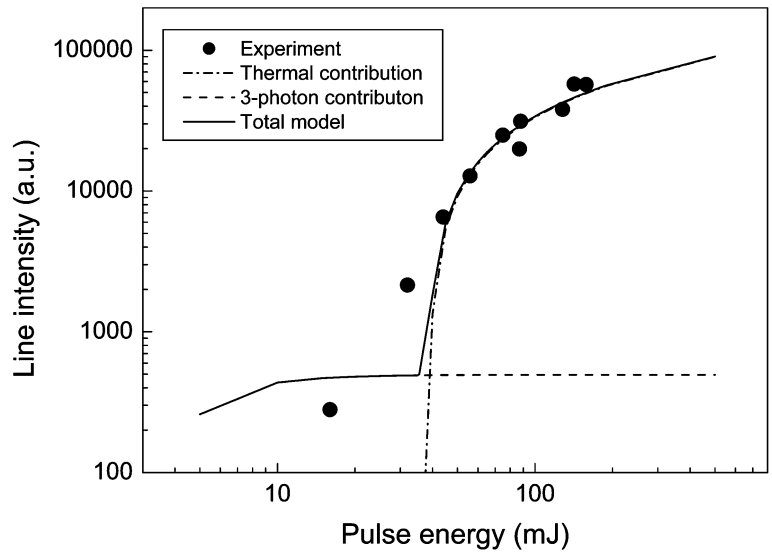

Fig. 8 Intensity of the copper 521.8 nm line induced by femtosecond pulse as a function of laser pulse energy. The experimental data are fitted to the model proposed by Hashida *et al.* The two significant processes contributing to the fit are also presented.

samples, spectra were recorded around 520 nm as a function of the chirp. The pulse duration that we investigated ranged from 75 fs to about one picosecond.

The obtained results are presented in Fig. 9: the intensities of the copper 521.8 nm line are shown in Fig. 9(a) and those of the AlO $B\,^2\Sigma^+ \rightarrow X\,^2\Sigma^+$, $\Delta v = -1$ line in Fig. 9(b). The pulse duration used in the figures are those on the sample. The GVD (group velocity dispersion) effect in air over the 25 m propagation distance are taken into account. Such effect is to stretch a positively chirped pulse and to compress a negatively chirped one. The GVD in air can be calculated using the air dispersion property.[41] For a short propagation distance and a moderate pulse intensity (far from the focus, propagation considered as linear), pulse duration variation is proportional to the propagation distance and the dispersion of the group refractive index. Using the data from ref. 41, for the 16 nm spectral bandwidth of the used femtosecond pulses, we get a pulse duration variation of $\Delta\tau = 1.01 \times D$ (fs), with D the propagation distance in m, which leads to a stretching or a compression of 25 fs for positively or negatively chirped pulses.

With both samples, the chirp effect was clearly observed: for the same pulse duration, the line intensity is higher for a positive chirp (red first) than for a negative chirp. The Fourier transform-limited minimal duration pulse does not induce an optimal signal similar to the observation on a Rb vapor.[38,39] When the pulse duration is increased with an applied chirp, the LIBS signal increases. In particular, the LIBS signal increase is not symmetric with respect to the minimal duration pulse. Such dissymmetry excludes a pulse duration effect (or power/intensity effect for a fixed pulse energy). In the studied pulse duration range the ratio between the signals for positive and negative chirps is found at maximum to be about 6.5 for copper and 4.1 for aluminium. The observed chirp effect is also consistent with what we found for the energy dependence concerning the nonlinear nature of the plasma generation in the ultrashort and ultraintense pulse regime.

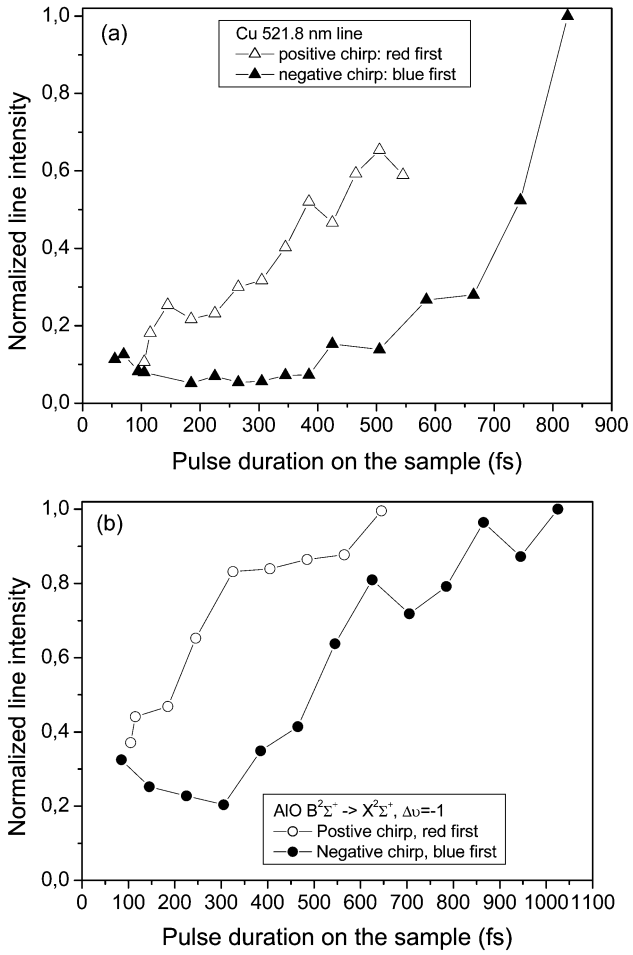

Fig. 9 Effect of the pulse chirp on the R-LIBS signals with femtosecond pulses. Normalized intensities of (a) the copper 521.8 nm and (b) the AlO $\Delta v = -1$ line as a function of the pulse duration. Data for different chirps (positive or negative) are presented in two different branches in each figure. Pulse durations refer to those on the sample. Pulse stretching or compression due to the GVD (group velocity dispersion) in air over the 25 m propagation distance are taken into account.

The chirp effect in optimising the fluorescence yield from a quantum system has been previously observed in atomic or molecular systems.[38,39] For such simple systems, the interpretation is based on a multiphoton transition *via* an intermediary level (situated out off the exact middle position from the fundamental to the excited level). With a properly designed pulse temporal-spectral shape, one can first induce a transition from the fundamental to the intermediary level with the first arrived spectral components. Then the delayed spectral components subsequently excite the transition from the intermediary level to the excited state. For a complicated process such as LIBS on solid state materials, new theoretical models are needed to describe in detail the mechanism.

The observed chirp effect appears very important for Femto-LIBS applications. It opens the perspective for optimising the fluorescence signal according to a specific sample or even a specific emission line. Such a material-dependent optimisation process is not only crucial for increasing the detection sensitivity, but also could be a powerful means to enhance the specificity of Femto-LIBS detection in the case, for example, of overlapping between the spectra of several elements to be identified.

4 Conclusion

We have demonstrated R-LIBS with metallic samples (cooper and aluminium). Our measurements showed that the LIBS spectra in the femtosecond and picosecond regimes with a high signal to noise ratio and a low background can be successively detected at a remote distance. In particular, femtosecond pulses induce a cleaner spectrum independent of the ambient gas. Moreover the high signal to noise ratio of recorded signals would allow us to detect as little as 100 ng of copper from a sample at a distance of 25 m.

Femtosecond as well as picosecond pulse induced fluorescence has been found to decay slowly with a time constant of several μs. Such long fluorescence lifetimes allows the application of standard gated detectors and have a long integration time. The secondary air plasma induced in the vicinity of the sample surface would provide a sensitive chemical analysis method for the ambient air.

The dependences on pulse energy and pulse chirp have been studied revealing interesting properties. The energy dependence has been found to be nonlinear and fits well to the model developed by Hashida *et al.*[18] As we can expect for a nonlinear optic process, an effect of the pulse chirp has been observed on the LIBS signal. The evidence of this effect has been provided in our experiments by a dissymmetrical LIBS signal increasing with respect to the minimal pulse duration. Our results show clearly that an intense femtosecond pulse with Fourier transform-limited minimal duration does not optimise the fluorescence signal. Instead a material-dependent optimisation process with a specific pulse shape would lead to a more efficient and more selective Femto-LIBS detection. Such improvements promise a longer detection distance for R-LIBS, as well as a high selectivity in the case of overlapping emission of various elements.

Our data does not only provide necessary parameters for the design of new LIBS devices with femtosecond or picosecond lasers, but also an experimental database for the establishment

of models describing the mechanisms involved in the LIBS process in such a new interaction regime with ultrashort and ultraintense laser pulses.

The application of the R-LIBS using ultra-short laser pulses would interest a large area covering for example, environmental monitoring (air, water or soil pollutions, heavy metal contamination…); *in-situ* and real time element detection and analysis of hazardous materials in difficult-access environments (high-temperature, radioactive, chemically toxic materials); mineral resource inspection; civil security and military defence (chemical, biological or nuclear contaminations…); and space missions. All these applications acquire a large detection distance using a mobile unit containing the laser system and the detection system. The need of scanning over a large detection area would be satisfied by the development of a motorised beam steering system, which would be synchronized with the orientation of the receiving telescope, in order to keep the alignment of the telescope at the laser beam impact on the targets. Starting from a versatile laser-detection unit such as the Teramobile system, engineering developments are certainly required to achieve a task-specified unit designed for a special application. Improvements in terms of the compactness of the system, the detection distance and the detection sensitivity can be expected.

Acknowledgements

This work has been performed within the framework of the Teramobile project, jointly funded by the French CNRS and the German DFG, and the French and the German Ministries of Research and of Foreign Affairs.

References

1 L. J. Radziemski, *Microchem. J.*, 1994, **50**, 218–234.
2 L. J. Radziemski and D. A. Cremers, Spectrochemical analysis using laser plasma excitation, in *Laser-induced Plasma: Physical, Chemical and Biological Applications*, ed. L. J. Radziemski and D. A. Cremers, Marcel Dekker, New York, 1989.
3 D. A. Rusak, B. C. Castle, B. W. Smith and J. D. Winefordner, *Crit. Rev. Anal. Chem.*, 1997, **27**, 257–290.
4 I. Schechter, *Rev. Anal. Chem.*, 1997, **16**, 173–298.
5 For a recent review of the fundamentals as well as applications of LIBS, see the special issue on laser-induced plasma spectroscopy, *Spectrochim. Acta, Part B*, 2002, **56**(6), 565–1034.
6 S. Palanco, S. Conesa and J. J. Laserna, Field deployable or remote enabled? A portable laser-induced plasma spectrometer for field remote sensing, paper Th-B2, ENSLIBS II, Hersonissos, Crete, Greece, 30 September–3 October 2003.
7 K. Kincade, *Laser Focus World*, 2003, **39**(8), 71–80.
8 D. Body and B. L. Chadwick, *Rev. Scient. Instrum.*, 2000, **72**, 1625–1629.
9 An introduction to laser-induced breakdown spectroscopy, Information from APPLIED PHOTONICS and BNFL Instruments, http://www.bnflinstruments.com/products/libs.pdf.
10 R. M. Measures, in *Laser Remote Sensing*, Wiley, New York, 1992.
11 R. J. Locke, J. B. Morris, B. E. Forch and A. W. Miziolek, *Appl. Opt.*, 1990, **29**, 4987–4992.
12 G. W. Rieger, M. Taschuk, Y. Y. Tsui and R. Fedosejevs, *Appl. Spectrosc.*, 2002, **56**, 689–698.
13 D. N. Stratis, K. L. Eland and S. M. Angel, *Appl. Spectrosc.*, 2002, **55**, 1297–1303.
14 R. Noll, R. Sattmann, V. Sturm and S. Winkelmann, Space- and time-resolved dynamics of plasmas generated by laser double pulses interacting with metallic samples, paper W-A1, ENSLIBS II, Hersonissos, Crete, Greece, 30 September–3 October 2003.
15 M. Corsi, G. Cristoforetti, M. Giuffrida, M. Hidalgo, S. Legnaioli, V. Palleschi, A. Salvetti, E. Tognoni and C. Vallebona, Spatially resolved analysis of single and double pulse laser induced plasma from a brass sample, paper W-A2, ENSLIBS II, Hersonissos, Crete, Greece, 30 September–3 October 2003.
16 See, for example: J. Kruger and W. Kautek, *Laser Phys.*, 1999, **9**, 30–40.
17 H. Furukawa and M. Hashida, *Appl. Surf. Sci.*, 2002, **197–198**, 114–117.
18 M. Hashida, A. F. Semerok, O. Gobert, G. Petit, Y. Izawa and J.-F. Wagner, *Appl. Surf. Sci.*, 2002, **197–198**, 862–867.
19 F. Brunner, T. Sudmeyer, E. Innerhofer, R. Paschotta, F. Morier-Genoud, U. Keller, J. Gao, K. Contag, A. Giesen, V. Kisel, V. G. Shcherbitsky and N. V. Kuleshov, 240-fs pulses with 22-W average power from a passively mode-locked thin-disk Yb:$KY(WO_4)_2$ laser'', in *Techn. Digest Conf. Laser Electro-Opt.*, Optical Society of America, Washinton DC, 2002, paper no. 02CH37337, 24 vol. 1.
20 A. Isemann, H. Hundertmark and C. Fallnich, *Appl. Phys. B*, 2002, **74**, 299–306.
21 T. Ueda, V. Yashin, M. Wakamatsu and A. Andreev, *Trans. Inst. Electr. Eng. Jpn., E*, 2002, **122**(5), 244–248.
22 K. L. Eland, D. N. Stratis, T. Lai, M. A. Berg, S. R. Goode and S. M. Angel, *Appl. Spectrosc.*, 2001, **55**, 279–285.
23 K. L. Eland, D. N. Stratis, D. M. Gold, S. R. Goode and S. M. Angel, *Appl. Spectrosc*, 2001, **55**, 286–291.
24 For a review of the results obtained by the Teramobile team, see for example: J. Kasparian, M. Rodriguez, G. Méjean, J. Yu, E. Salmon, H. Wille, R. Bourayou, S. Frey, Y.-B. André, A. Mysyrowicz, R. Sauerbrey, J.-P. Wolf and L. Wöste, *Science*, 2003, **301**, 61–64.
25 H. Wille, M. Rodriguez, J. Kasparian, D. Mondelain, J. Yu, A. Mysyrowicz, R. Sauerbrey, J.-P. Wolf and L. Wöste, *Eur. Phys. J. A*, 2002, **20**, 183–190.
26 D. Strickland and G. Mourou, *Opt. Commun.*, 1985, **56**, 219–221.
27 I. G. Dors, C. Parigger and J. W. Lewis, *Opt. Lett.*, 1998, **23**, 1778–1781.
28 B. Le Drogoff, F. Vidal, Y. von Kaenel, M. Chakern, T. W. Johnston, S. Laville, M. Sabsabi and J. Margot, *J. Appl. Phys.*, 2001, **89**, 8247–8252.
29 A. Ng, D. Pasini, P. Celliers, D. Parfenuik, L. Da Silva and J. Kwan, *Appl. Phys. Lett.*, 1984, **45**, 1046–1048.
30 F. Dahmani, *J. Appl. Phys.*, 1993, **74**, 622–634.
31 The NIST spectral databass is available at the website: http://physics.nist.gov/cgi-bin/AtData/main_asd.
32 S. S. Mao, Xianglei Mao, Ralph Greif and Richard E. Russo, *Appl. Phys. Lett.*, 2000, **77**, 2464–2466.
33 K. Shigemori, H. Azechi, M. Nakai and K. Mima, *Rev. Sci. Instrum.*, 1998, **69**, 3942–3944.
34 C. H. Ching, R. M. Gilgenbach and J. S. Lash, *J. Appl. Phys.*, 1995, **78**, 3408–3410.
35 S. M. Angel, D. N. Stratis, K. L. Eland, T. Lai, M. A. Berg and D. M. Gold, *Fresenius' J. Anal. Chem.*, 2001, **369**, 320–327.
36 S. Tzortzakis, B. Prade, M. Franco and A. Mysyrowicz, *Opt. Commun.*, 2000, **181**, 123–127.
37 D. Meshulach and Y. Silberberg, *Nature*, 1998, **396**, 239–242.
38 B. Chatel, J. Degert, S. Stcok and B. Girad, *Phys. Rev. A*, 2003, **68**, 41402(R).
39 N. Dudovich, B. Dayan, S. M. Gallagher Faeder and Y. Silberberg, *Phys. Rev. Lett.*, 2001, **86**, 47–50.
40 R. Stoian, M. Boyle, A. Thoss, A. Rosenfeld, G. Korn, I. V. Hertel and E. E. B. Campbell, *Appl. Phys. Lett.*, 2002, **80**, 353–355.
41 J. C. Owens, *Appl. Opt.*, 1967, **6**, 51–59.